Australas Phys Eng Sci Med
DOI 10.1007/s13246-017-0579-6

SCIENTIFIC PAPER

Measurement of dose in radionuclide therapy by using Cerenkov radiation

Yao Ai[1] · Xiaobin Tang[1,2] · Diyun Shu[1] · Wencheng Shao[1] · Chunhui Gong[1] · Changran Geng[1,2] · Xudong Zhang[1] · Haiyan Yu[1]

Received: 24 March 2017 / Accepted: 6 August 2017

Abstract This work aims to determine the relationship between Cerenkov photon emission and radiation dose from internal radionuclide irradiation. Water and thyroid phantoms were used to simulate the distribution of Cerenkov photon emission and dose deposition through Monte Carlo method. The relationship between Cerenkov photon emission and dose deposition was quantitatively analyzed. A neck phantom was also used to verify Cerenkov photon detection for thyroid radionuclide therapy. Results show that Cerenkov photon emission and dose deposition exhibit the same distribution pattern in water phantom, and this relative distribution relationship also existed in the thyroid phantom. Moreover, Cerenkov photon emission exhibits a specific quantitative relation to dose deposition. For thyroid radionuclide therapy, only a part of Cerenkov photon produced by thyroid could penetrate the body for detection; therefore, the use of Cerenkov radiation for measurement of radionuclide therapy dose may be more suitable for superficial tumors. This study demonstrated that Cerenkov radiation has the potential to be used for measuring radiation dose for radionuclide therapy.

Keywords Cerenkov radiation · Radionuclide therapy · Internal radiation · Dosimetry

✉ Xiaobin Tang
tangxiaobin@nuaa.edu.cn

[1] Department of Nuclear Science and Engineering, Nanjing University of Aeronautics and Astronautics, 29 Yudao St., Nanjing 210016, China

[2] Collaborative Innovation Center of Radiation Medicine of Jiangsu Higher Education Institutions, 29 Yudao St., Nanjing 210016, China

Introduction

Radionuclide therapy is firmly established as an effective treatment modality, which is expanding via the introduction of new radionuclides, new carrier molecules, and combination with other therapies. In radionuclide therapy, killing malignant cells to treat a disease is difficult when the dose administered to the target area is insufficient. Moreover, normal tissues and organs adjacent to the target area may suffer from radiation hazards if the target area is overdosed. These adverse consequences due to dose differences can be resolved by dosimetry methods.

Three dosimetry methods are used for radionuclide therapy, including Medical Internal Radiation Dose (MIRD) dosimetry [1], dose-point kernel convolution dosimetry [2], and patient-specific Monte Carlo method [3]. MIRD method estimates the average absorbed dose for the organ or tumor in the region of interest. The two other methods can produce a detailed absorbed dose distributions, the underlying processes are complex and time consuming [4, 5].

However, there is currently no efficient method to directly measure the radiation dose during treatment for both purposes of quality assurance and treatment optimization.

Cerenkov radiation are photons emitted by charged particles transported in a dielectric medium at a speed greater than the phase velocity of light in that medium. In recent years, Cerenkov radiation has been researched extensively for potential applications in life sciences and engineering. A number of articles have introduced its potential application in accelerator beam monitoring [6], external radiotherapy dosimetry [7–9], and molecular imaging [10–13]. However, studies on the relationship between Cerenkov photon emission and the radiation dose from internal radionuclide are limited. Cerenkov radiation as a potential dosimetry method

Published online: 14 August 2017

for radionuclide therapy has the advantage of low cost and easy operation compared with the traditional method [14].

In this study, three different radionuclides (^{131}I, ^{32}P, and ^{90}Y) were selected to determine the relationship between the Cerenkov photon emission and dose deposition, and the Geant4 Monte Carlo toolkit was used to perform Monte Carlo simulations of treatment and radiation transportation. The water phantom was used to quantitatively analyze the relationship between the Cerenkov photon emission and dose deposition under different radionuclide distributions. Moreover, a complex distribution of radionuclide in thyroid was also studied based on a hybrid human phantom to determine the potential influencing factors for a patient case.

Materials and methods

Cerenkov radiation

The Cerenkov effect is a well-known phenomenon that occurs when a charged particle travels through a medium with a velocity greater than the speed of light in the medium. The charged particle can come from outside the medium but can also be generated within the medium, such as radionuclide decay, γ-ray, and other uncharged particles produce secondary charged particles in the medium.

The threshold energy of a charged particle with rest mass m_0 to generate Cerenkov radiation in a medium is given by

$$E_T = m_0 c^2 \left[\frac{n}{(n^2-1)^{1/2}} - 1 \right]$$

where n and c represent the refractive index of the medium and the speed of light, respectively. For example, the threshold energies of an electron to generate Cerenkov radiation in water ($n = 1.33$) and muscle ($n = 1.4$) are 0.263 and 0.219 MeV, respectively. Therefore, most of the beta plus and minus emitted by radionuclides commonly used in molecular imaging, diagnosis, and treatment have end point energies greater than the Cerenkov threshold in the tissues.

Virtual water phantom

Geant4 toolkit (version 4.10.1.p01) [15, 16] was employed to simulate particle transport and analyze the relationship between Cerenkov photon emission and internal dose in radionuclide therapy. The standard low-energy electromagnetic physical process and the optical physical process were used, and the cut-off value was set to 0.01 mm. For each simulation, the number of radionuclide decays was set to 1×10^9. Three representative radionuclides (^{131}I, ^{32}P, and ^{90}Y), which emit beta-minus particles with 0.6, 1.7, and 2.2 MeV end-point energy, for nuclear medicine were selected in this study. A $5 \times 5 \times 5$ cm^3 cubic phantom was constructed, and a sphere with a radius of 1.5 cm containing radionuclide was embedded in the center. Water was chosen as the tissue equivalent material in both of the two geometric models, as shown in Fig. 1. The Cerenkov photon emission and dose deposition along the radial direction of the sphere were tallied.

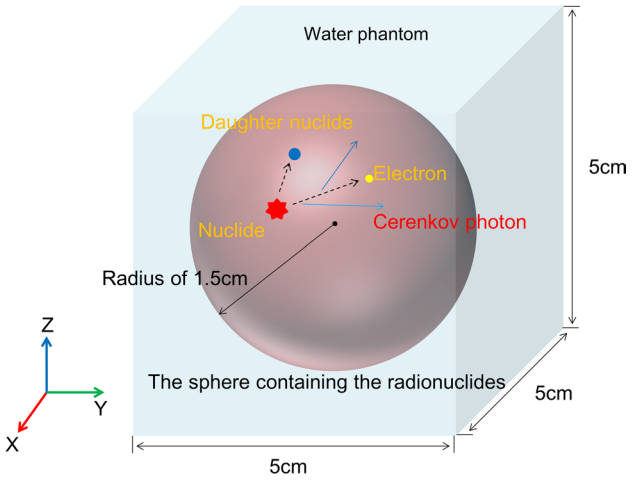

Fig. 1 Geometric setup for water phantom

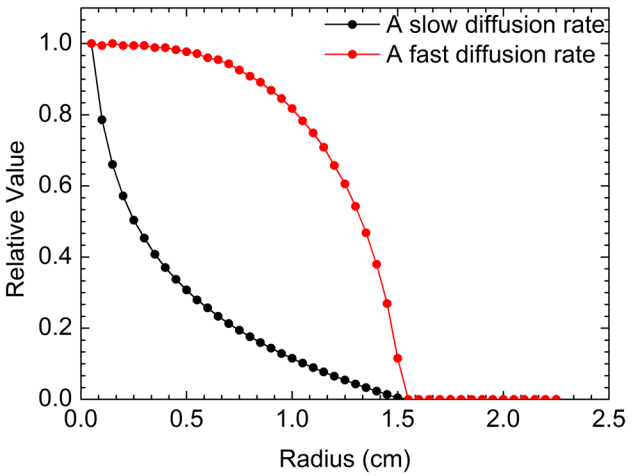

Fig. 2 Distribution of radionuclide activity in water phantom

Ideally, radionuclides are uniformly distributed when the therapeutic radionuclides are injected into the tumor. However, the diffusion rate of radionuclides within the tumor varies depending on the type of the tumor. Therefore, two different distributions of radionuclide were assumed; as illustrated in Fig. 2, the black and red curves respectively represent the radionuclide activity distribution in the sphere when the radionuclide was diffused at a slow rate and a fast rate.

Neck voxel phantom

To simulate the distribution of radionuclide in lesions more realistically, a neck voxel phantom with optical properties was established based on the 30-year-old CHRP-Female [17]. The voxel resolution was $0.2 \times 0.2 \times 0.2$ mm^3, as shown in Fig. 3. The compositions of this organ were from ICRU-46 and ICRP-89 [18, 19]. The distance from the skin surface to the thyroid was approximately 1 cm. Optical properties, such as scattering and attenuation coefficients, obtained from the literature were applied to each tissue and organ. Optical characterization of the soft tissue, skin, and the muscle can be found in the study of Bashkatov [20, 21]. Given that the thyroid has a similar density to the muscles, the thyroid is assumed to have the same optical properties as the muscles. A constant refractive index of $n = 1.4$ was assumed for all wavelengths due to lack of available date for all voxels of the phantom [22, 23].

To obtain an ideal treatment effect to thyroid disease, the ideal condition of radionuclides ^{131}I should be uniformly distributed in the thyroid so that each part would get the same radiation dose. However, iodine absorption varies in different parts of the thyroid gland, generating the high-radioactivity region and low-radioactivity region of iodine. To simulate the distribution of ^{131}I in the high and low-concentration regions in the thyroid, a radioactive "cold area" and "hot area" were set up in the lower part of the right lobe and the upper part of the left lobe respectively, as illustrated in Fig. 4.

The detection of Cerenkov radiation in the treatment of thyroid diseases with radionuclide was also studied. A detector array with a length of 15×15 cm^2 was set up outside the neck to record the Cerenkov photons from the thyroid, and the distance from the skin surface to the array was approximately 3 mm, as shown in Fig. 3.

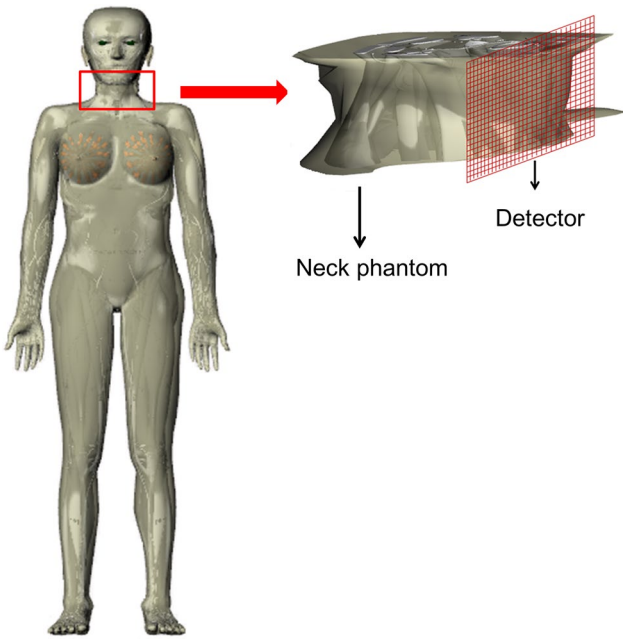

Fig. 3 Demonstration of the detection of Cerenkov photons outside of the neck phantom using a virtual two-dimensional detector array (*red grids*)

Results

Cerenkov photon emission and dose deposition for uniformly distributed radionuclides in the water phantom

The relationship between Cerenkov photon emission and dose in the radial direction is plotted in Fig. 5a–c for ^{131}I, ^{32}P, and ^{90}Y uniformly distributed in the water phantom. The Cerenkov photon emission and dose were normalized to their maximum values. As shown in the curves, the relative Cerenkov photon emission was consistent with the corresponding dose values for ^{131}I, ^{32}P, and ^{90}Y. For the radius larger than 1.5 cm, the Cerenkov photon emission and dose decreased rapidly, and the differences between Cerenkov photon emission and dose appeared at the edge of radionuclide concentrated region. The differences between the Cerenkov photon emission and dose are less than 1.1, 2.3, and 2.1% for ^{131}I, ^{32}P, and ^{90}Y, respectively.

The radionuclide ^{90}Y was selected to explore the two-dimensional distribution of the Cerenkov photon emission and the dose in water phantom, as shown in Fig. 6a, b. The distributions of Cerenkov photon emission and the dose were similar to each other, and clear dose outlines appeared along the border of the ^{90}Y concentrated region. In the central region of the sphere, uniform distributions were observed for Cerenkov photon emission and the dose.

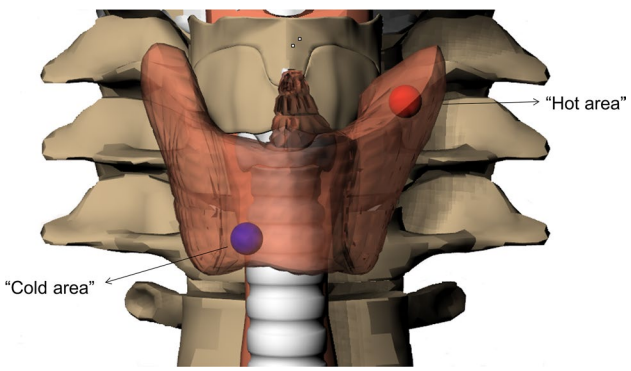

Fig. 4 The thyroid phantom contains a "cold area" and "hot area"

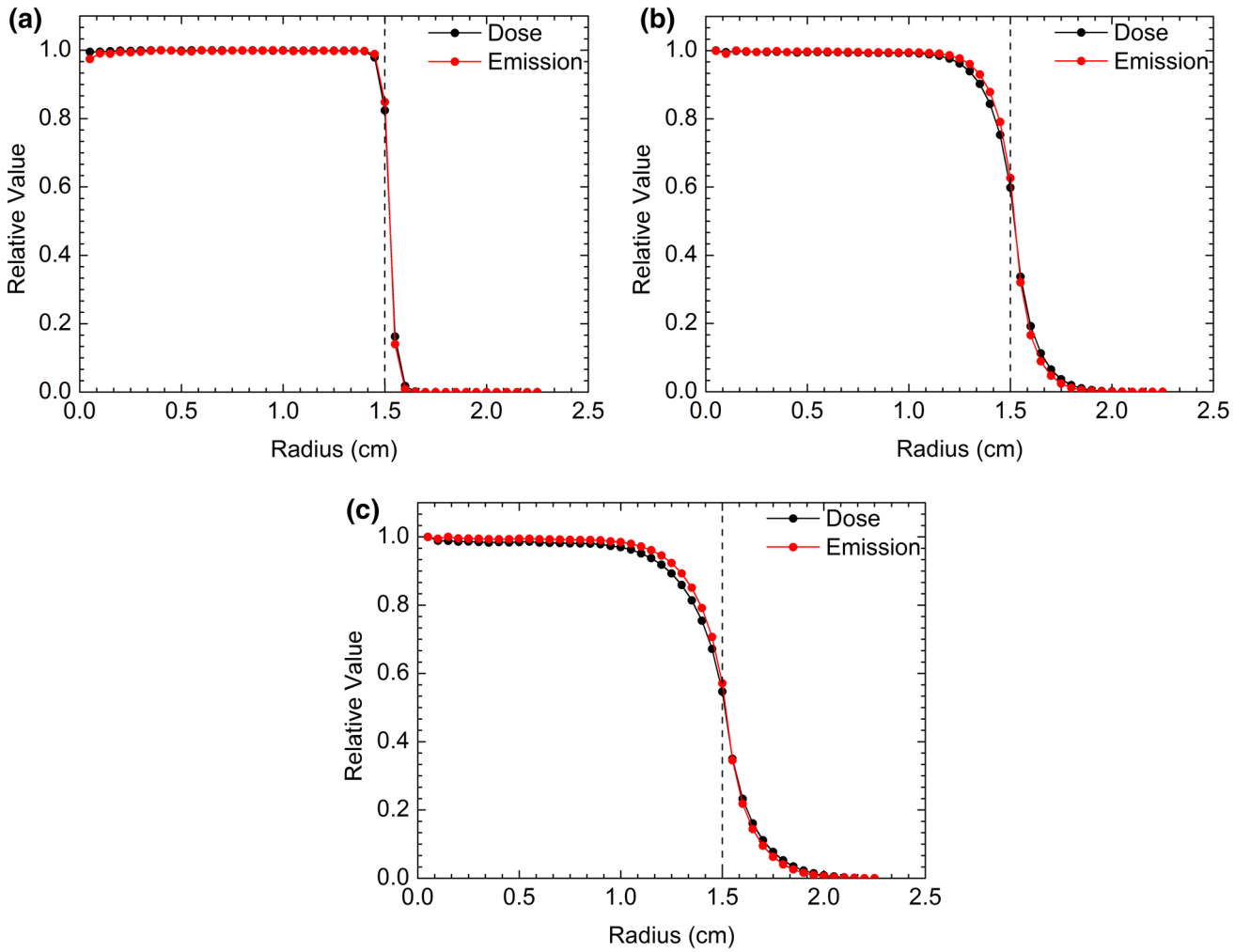

Fig. 5 Relative Cerenkov photon emission and dose deposition for ^{131}I (**a**), ^{32}P (**b**), and ^{90}Y (**c**)

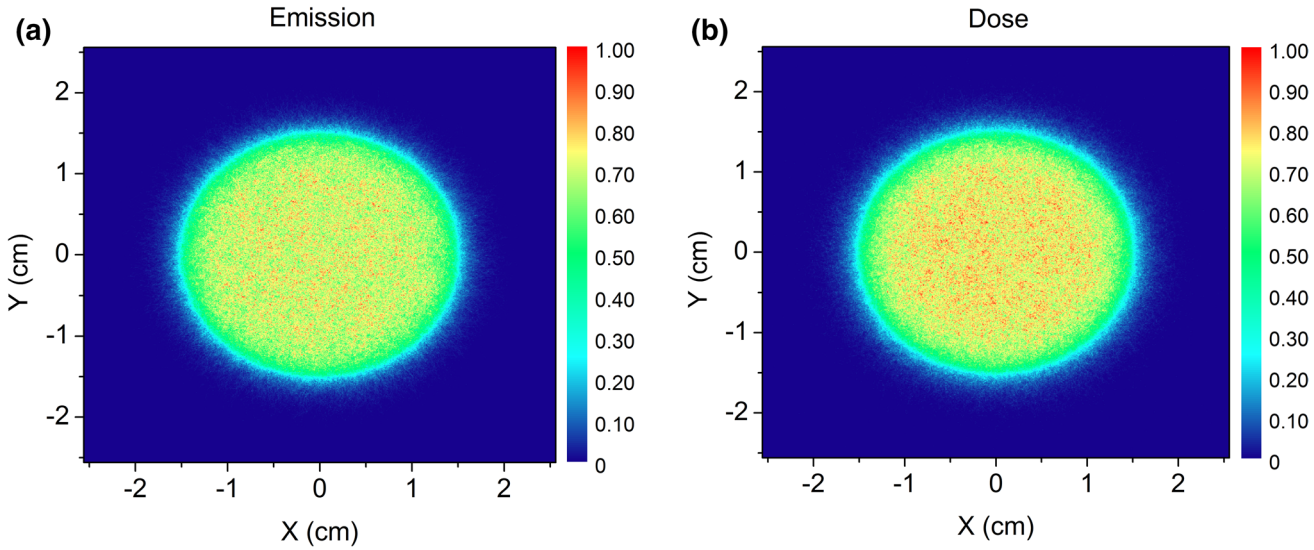

Fig. 6 Two-dimensional distribution of Cerenkov photon emission (**a**) and dose deposition (**b**) produced by ^{90}Y

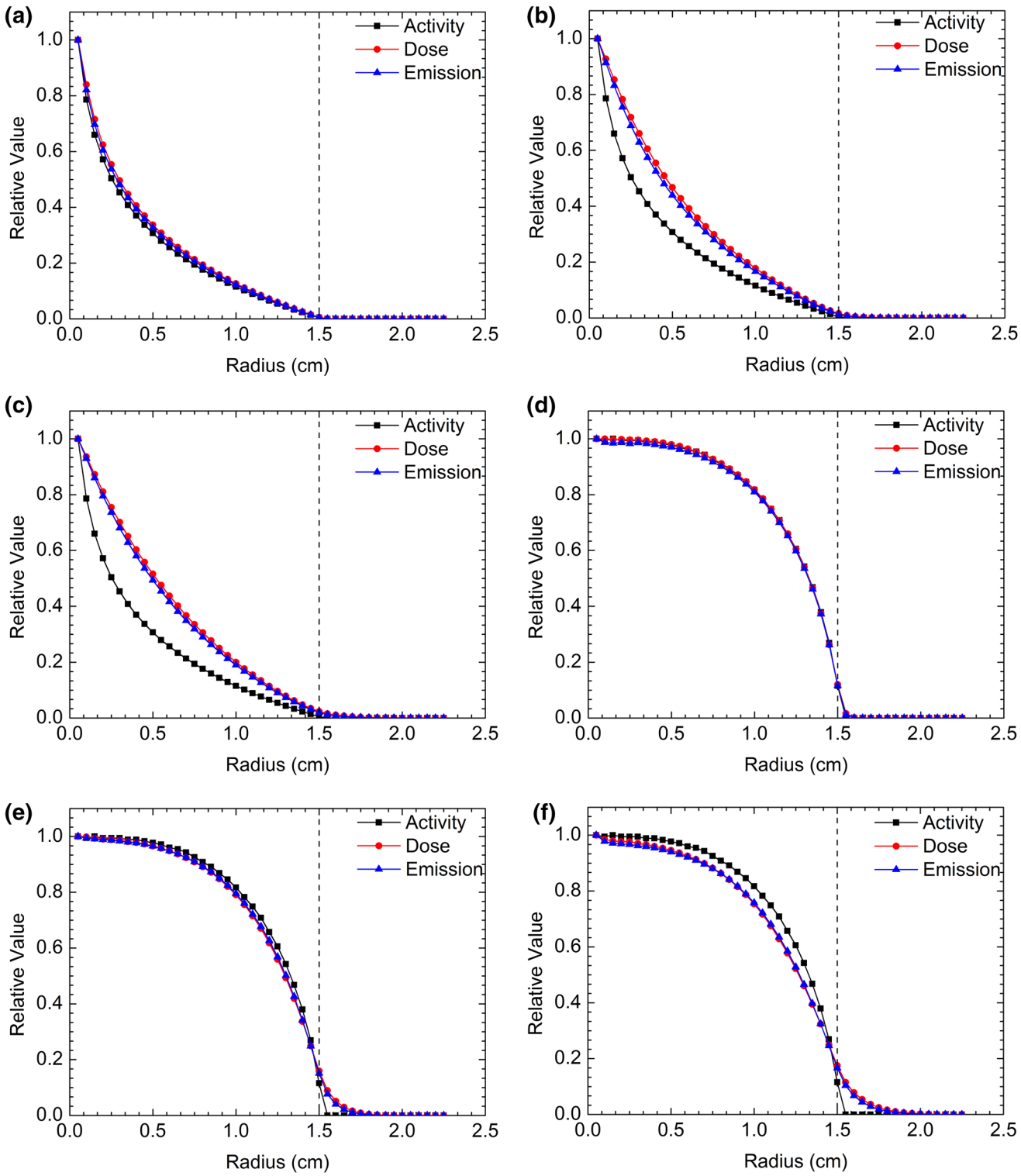

Fig. 7 Relative Cerenkov photon emission and dose deposition for ^{131}I (**a**), ^{32}P (**b**), and ^{90}Y (**c**) with a slow diffusion rate. Relative Cerenkov photon emission and dose deposition for ^{131}I (**d**), ^{32}P (**e**), and ^{90}Y (**f**) with a fast diffusion rate

Cerenkov photon emission and dose deposition for nonuniformly distributed radionuclides in the water phantom

Figure 7a–c show the relative Cerenkov photon emission and dose curves in the radial direction produced by three radionuclides ^{131}I, ^{32}P, and ^{90}Y with a slow diffusion rate, and Fig. 7d–f present the result with a fast diffusion rate. The black curve in each figure represents the relative distribution of radionuclide activity in the radial direction. The Cerenkov photon emission and dose were normalized to their maximum values for all cases. The results show that the Cerenkov photon emission and dose have the same trend in these two distributions for these radionuclides. For ^{131}I, ^{32}P, and ^{90}Y, the differences between the Cerenkov photon emission and dose are less 0.3, 3.5, and 4.0% for the slow diffusion rate; and 0.1, 0.9, and 1.2% for the fast diffusion rate.

Based on the distribution of the two radionuclide activity mentioned above, the radionuclide ^{90}Y was selected to explore the two-dimensional distribution of Cerenkov photon emission and dose. The two-dimensional distribution of the Cerenkov photon emission and dose with a slow diffusion rate can be seen in Fig. 8a–b, and Fig. 8c–d show the results with a fast diffusion rate.

Quantitative relationship between the Cerenkov photon emission and dose deposition

The relationship between the Cerenkov photon emission (i.e., N_C) and dose deposition (i.e., *Dose*) within the irradiated medium, can be defined as the total number of photons

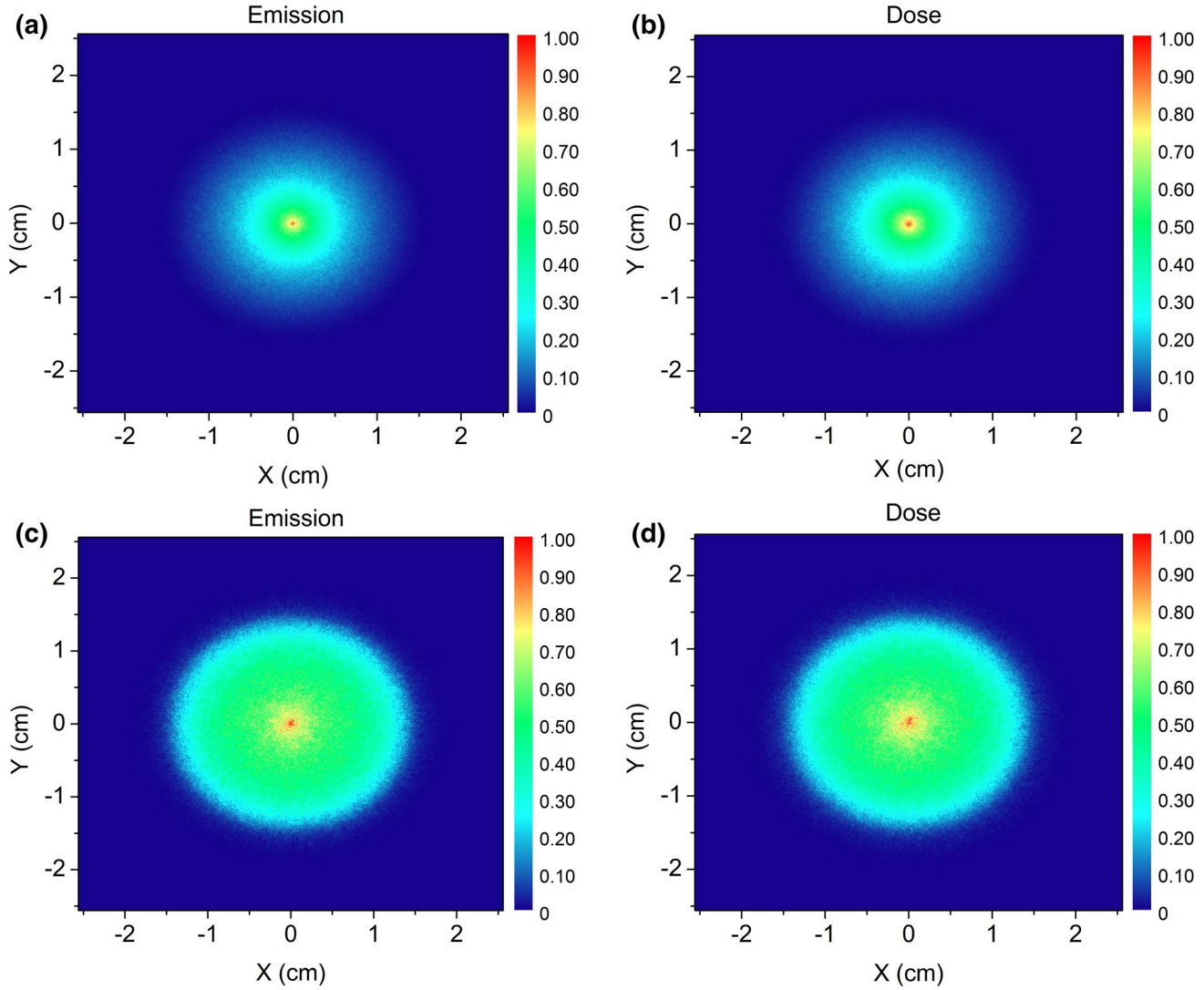

Fig. 8 Two-dimensional distribution of Cerenkov photon emission (**a**) and dose deposition (**b**) produced by ^{90}Y with a slow diffusion rate. Two-dimensional distribution of Cerenkov photon emission (**c**) and dose deposition (**d**) produced by ^{90}Y with a fast diffusion rate

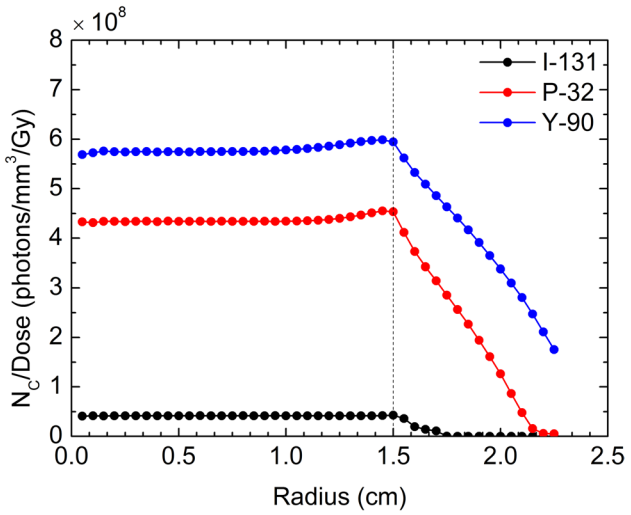

Fig. 9 *R* values in the radial direction produced by ^{131}I, ^{32}P, and ^{90}Y with uniform distribution

emitted by the Cerenkov effect at any given spatial location to the amount of dose deposited at that same spatial location, $R = N_C/Dose$ [7].

When the three kinds of radionuclide (^{131}I, ^{32}P, and ^{90}Y) were uniformly distributed in the water phantom, the relationship between the Cerenkov photon emission and dose deposition in the radial direction was shown in Fig. 9. The *R* values almost kept as the constants in the radionuclide-concentrated regions, where radius is smaller than 1.5 cm. The *R* values for ^{131}I, ^{32}P, and ^{90}Y were approximate to 4.1×10^7 (photons/mm^3/Gy), 4.3×10^8 (photons/mm^3/Gy), and 5.7×10^8 (photons/mm^3/Gy), respectively. However, the *R* values gradually decrease for outside the radionuclide-concentrated regions.

Considering the radionuclide distributed in the water phantom with a slow and fast diffusion rate. Figure 10 shows the relationships between the Cerenkov photon emission and dose deposition in the radial direction for the considered three kinds of radionuclide (^{131}I, ^{32}P, and ^{90}Y). Figure 10a, b show that whether the diffusion rate is slow or fast, the *R* values were approximately 4.1×10^7 (photons/mm^3/Gy), 4.3×10^8 (photons/mm^3/Gy), and 5.7×10^8 (photons/mm^3/Gy) for ^{131}I, ^{32}P, and ^{90}Y in the radionuclide-concentrated regions, which was same as the relationship for the case of uniform distribution. In addition, the *R* values also gradually decreased outside the radionuclide-concentrated.

Distribution of Cerenkov photon emission and dose deposition in thyroid phantom

Figure 11a, b show the two-dimensional distribution of Cerenkov photon emission and absorbed dose at the transverse plane in the case of nuclide uniformly distributed in the thyroid. It is evident that the Cerenkov photons and the dose have similar two-dimensional distribution in the thyroid phantom, and both were uniformly distributed.

Figure 12a, b show the two-dimensional distribution of Cerenkov photon emission and dose at the transverse plane in the "cold area", and Fig. 12c, d show the results in the "hot area". The Cerenkov photon emission and the dose have the similar two-dimensional distribution in the "cold area" and "hot area".

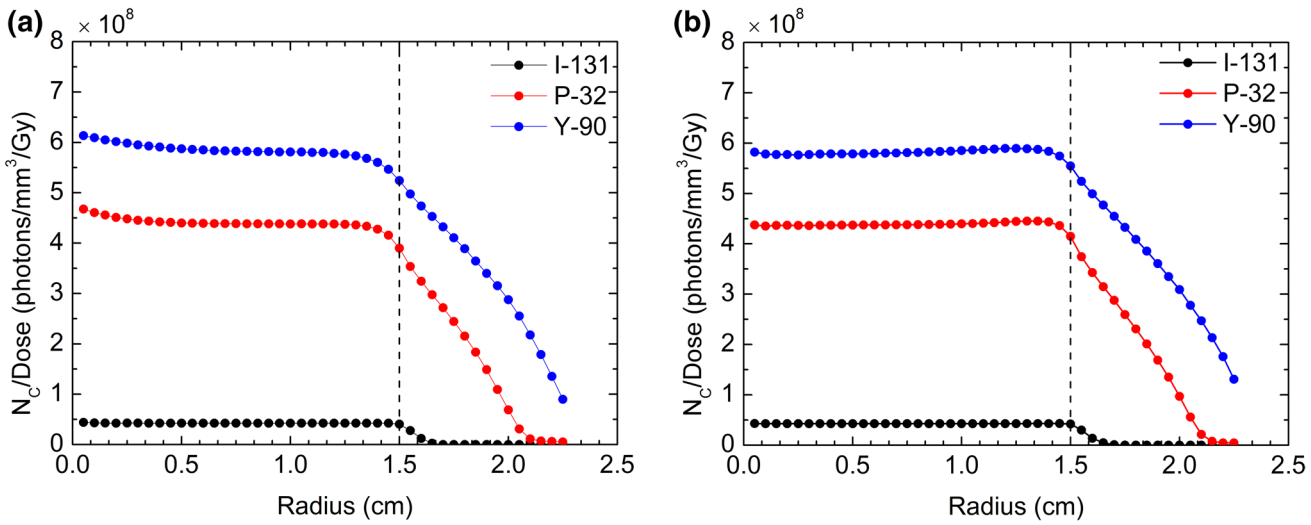

Fig. 10 *R* values in the radial direction produced by ^{131}I, ^{32}P, and ^{90}Y with a slow diffusion rate (**a**). *R* values in the radial direction produced by ^{131}I, ^{32}P, and ^{90}Y with a fast diffusion rate (**b**)

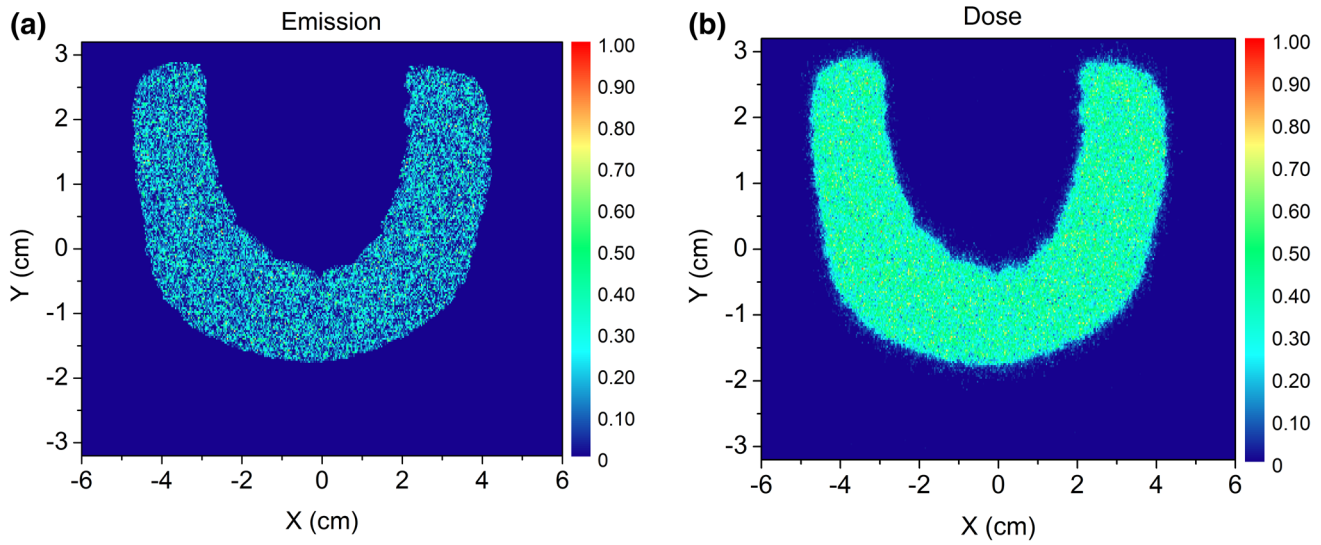

Fig. 11 Two-dimensional distribution of Cerenkov photon emission (**a**) and dose deposition (**b**) at the transverse plane in thyroid phantom

Simulation of the detection of Cerenkov radiation

Based on the human neck phantom, the relative intensity distribution of Cerenkov photons in vitro when radionuclide iodine is uniformly distributed in the thyroid phantom is shown in Fig. 13. The results show that the relative intensity distribution of Cerenkov photons can roughly reflect the profile of the thyroid, and the intensity of the Cerenkov photons in the central area of the thyroid was higher than at the edge.

Discussion

Radionuclide therapy is a promising method for treating malignant tumors. However, there is not an effective method for monitoring the radiation dose inside the tumor for radionuclide therapy. This study presents a novel dose monitoring method through detecting the Cerenkov photons emitted from the tumor during radionuclide therapy. The relationship between Cerenkov photon emission and absorbed dose from internal radionuclide was theoretically studied by Monte Carlo simulation. To some extent, the results of this study can serve as a fundamental basis for future research on real-time tumor dose monitoring in radionuclide therapy.

As illustrated in Figs. 5a–c and 7a–f, there is a good agreement between the Cerenkov photon emission and dose. As shown in Fig. 7a–f, compared with the distribution of radioactivity, the trend of the Cerenkov photon emission and the dose in the radial direction is similar to that of radioactivity, but the changing rate is different. The difference increases with increasing electron mean energies of the β-emitting radionuclides. This can be attributed to the larger mean energy of electrons that results in longer electron ranges compared to the smaller mean energy of electrons, and therefore, more electrons fled from high-concentration regions to low-concentration regions and deposited part of their energies in low-concentration regions.

Quantitative analysis of the relationship between Cerenkov photon emission and dose is critical to realize further application of Cerenkov radiation-based measurement of radionuclide therapy does in clinical practice. According to the study of Glaser [7], in order for a Cerenkov radiation based optical dosimetry method to be successful, R ideally is expected to be constant. As shown in Figs. 9 and 10, the relationship between the number of Cerenkov photon emission and dose in the radial direction is almost constant in the radionuclide-concentrated regions regardless of whether the radionuclide is uniformly or non-uniformly distributed. The values were approximately 4.1×10^7 (photons/mm^3/Gy), 4.3×10^8 (photons/mm^3/Gy), and 5.7×10^8 (photons/mm^3/Gy) for ^{131}I, ^{32}P, and ^{90}Y, respectively. For the same mean energy of the electron, the number of Cerenkov photons emitted is proportional to the locally deposited dose [24]; therefore, the R values remains unchanged for the same electron mean energies of the β-emitting radionuclides and was not related to the distribution. However, the R values gradually decreased outside the radionuclide-concentrated regions. This is due to the mean energy of electrons decreasing with increasing radius, and therefore, the number of electron with energies below the threshold for Cerenkov photon emission increased. They still deposited dose but did not contribute to the Cerenkov photon emission. As a result, the R value gradually decreases outside the radionuclide-concentrated regions in the radial direction.

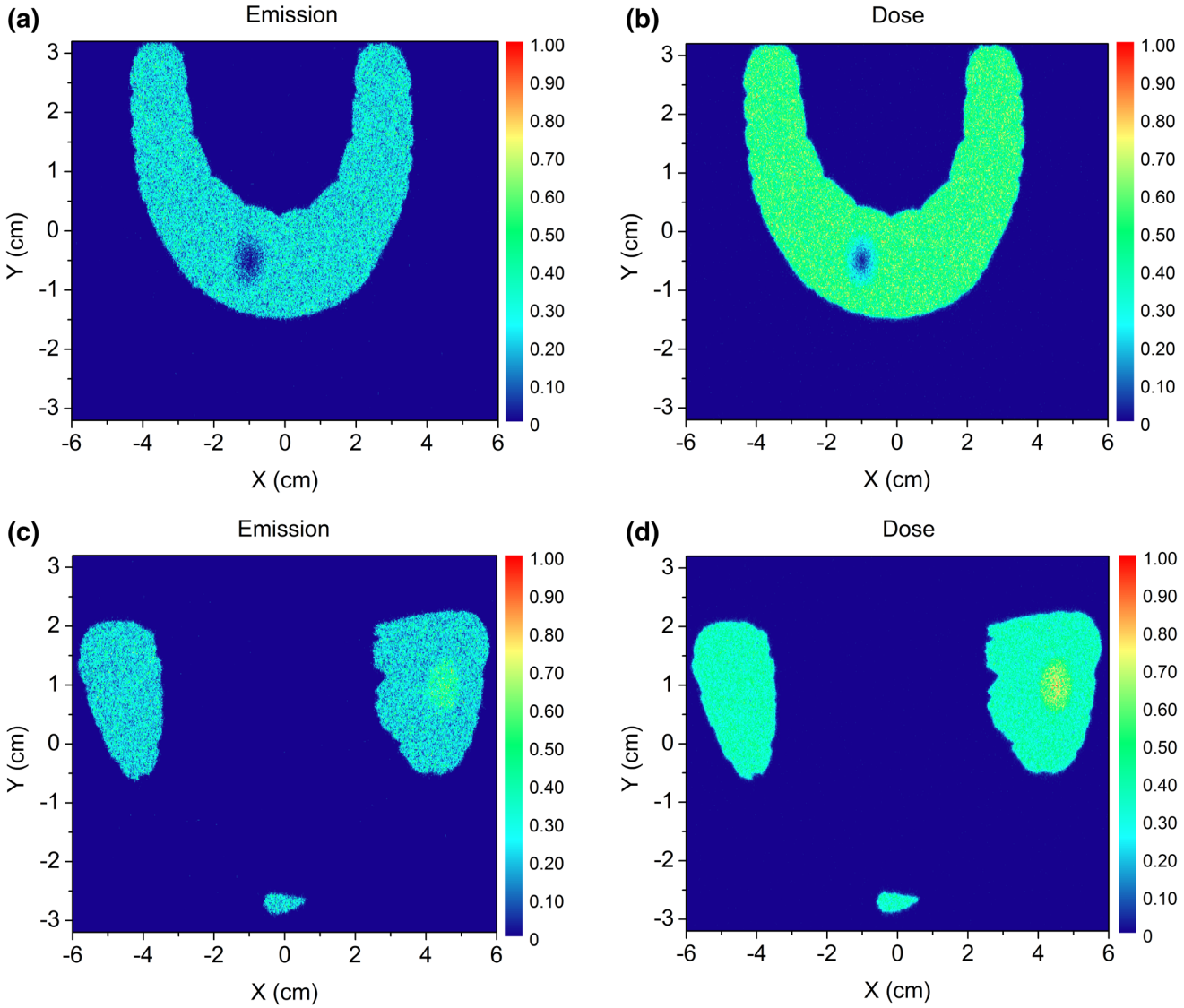

Fig. 12 Two-dimensional distribution of Cerenkov photon emission (**a**) and dose deposition (**b**) at the transverse plane in the "cold area". Two-dimensional distribution of Cerenkov photon emission (**c**) and dose deposition (**d**) at the transverse plane in the "hot area"

To explore the capability of the Cerenkov photon emission to accurately reflect the true dose distribution, a thyroid phantom was used to analyze the distribution of Cerenkov photon and dose. As shown in Fig. 12a–d, with existing "hot area" and "cold area" regions in the thyroid, the distribution of Cerenkov photon emission and the dose remains correlated. The dark and light spots in the distribution of Cerenkov photons are correlated to the location and size of the "cold area" and "hot area" of dose.

To detect the Cerenkov radiation, as a potential means of measuring dose (e.g., using an external CCD camera), the externally detected 2D distribution of Cerenkov photons can roughly reflect the profile of the thyroid (Fig. 13). Given that the Cerenkov photon produced in the deep tissue had difficulty to penetrate the tissue and skin, this part of photons was hard to detect. Therefore, the use of Cerenkov radiation for radionuclide therapy dose measurement might be more suitable for superficial tumors.

Given that there are numerous studies on Cerenkov dosimetry for external radiation therapy [25–28], the developed technology could be translated to internal radiation therapy based on our result. However, certainly more efforts are warranted for experimental studies (e.g., detection efficiency, resolution, clinical implementation, etc).

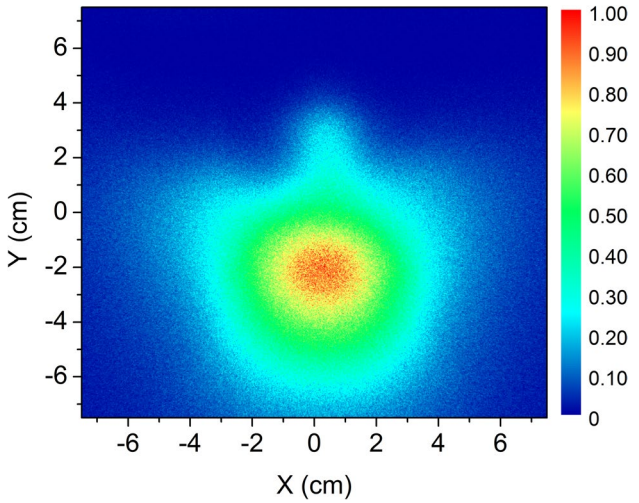

Fig. 13 Detection of Cerenkov photon in thyroid radionuclide therapy

Conclusion

In this study, we studied a potential method of measuring internal radiation dose with Cerenkov radiation. The results revealed the relationship and physical mechanism between the Cerenkov photon emission and dose in radionuclide therapy.

These theoretical simulations and the analytical interpretation of this method are useful for demonstrating the feasibility of using the Cerenkov radiation for measuring the internal dose for radionuclide therapy. However, the actual distribution of radionuclide was influenced by the tissue or organ absorption capacity and human metabolism, resulting in a complex distribution of radionuclide. Therefore, exploring the relationship between the Cerenkov photon emission and dose in complex and actual conditions is warranted.

Acknowledgements This work was supported by the National Natural Science Foundation of China (Grant No. 11475087), the National Key Research and Development Program (Grant No. 2016YFE0103600), the Foundation of Graduate Innovation Center in NUAA (Grant Nos. kfjj20160610, kfjj20170617), and the Priority Academic Program Development of Jiangsu Higher Education Institutions.

Compliance with ethical standards

Conflict of interest The authors declare that they have no conflict of interest.

Ethical approval This article does not contain any studies with human participants or animals performed by any of the authors.

References

1. Flower MA, Chittenden SJ (1993) Unsealed source therapy. In: Williams JR, Thwaiters DI (eds) Radiotherapy physics in practice. Oxford University Press, Oxford, pp 253–274
2. Giap HB, Macey DJ, Bayouth JE, Boyer AL (1995) Validation of a dose-point kernel convolution technique for internal dosimetry. Phys Med Biol 40:365–381
3. Furhang EE, Chui CS, Sgouros G (1996) A Monte Carlo approach to patient specific-dosimetry. Med Phys 23:1523–1529. doi:10.1118/1.597882
4. Rosenthal MS, Cullom J, Hawkins W, Moore SC, Tsui BMW, Yester M (1995) Quantitative SPECT imaging: a review and recommendations by the Focus Committee of the Society of Nuclear Medicine Computer and Instrumentation Council. J Nucl Med 36:1489–1513
5. Giap HB, Macey DJ, Podoloff DA (1995) Development of a SPECT-based three-dimensional treatment planning system for radioimmunotherapy. J Nucl Med 36:1885–1894
6. Glaser AK, Andreozzi JM, Davis SC, Zhang R, Pogue BW, Fox CJ, Gladstone DJ (2014) Video-rate optical dosimetry and dynamic visualization of IMRT and VMAT treatment plans in water using Cherenkov radiation. Med Phys 41:062102. doi:10.1118/1.4875704
7. Glaser AK, Zhang R, Gladstone DJ, Pogue BW (2014) Optical dosimetry of radiotherapy beams using Cherenkov radiation: the relationship between light emission and dose. Phys Med Biol 59:3789–3811. doi:10.1088/0031-9155/59/14/3789
8. Shu D, Tang X, Geng C, Gong C, Chen D (2016) Determination of the relationship between dose deposition and Cerenkov photons in homogeneous and heterogeneous phantoms during radiotherapy using Monte Carlo method. J Radioanal Nucl Chem 308:187–193. doi:10.1007/s10967-015-4316-x
9. Glaser AK, Davis SC, McClatchy DM, Zhang R, Pogue BW, Gladstone DJ (2013) Projection imaging of photon beams by the Čerenkov effect. Med Phys 40:012101. doi:10.1118/1.4770286
10. Volotskova O, Sun C, Stafford JH, Koh AL, Ma X, Cheng Z, Cui B, Partx G, Xing L (2015) Efficient radioisotope energy transfer by gold nanoclusters for molecular imaging. Small 11:4002–4008. doi:10.1002/small.201500907
11. Hu Z, Qu Y, Wang K, Zhang X, Zha J, Song T et al (2015) In vivo nanoparticle-mediated radiopharmaceutical-excited fluorescence molecular imaging. Nat commun. doi:10.1038/ncomms8560
12. Shimamoto M, Gotoh K, Hasegawa K, Kojima A (2016) Hybrid light imaging using Cerenkov luminescence and liquid scintillation for preclinical optical imaging in vivo. Mol Imaging Biol 18:500–509. doi:10.1007/s11307-016-0928-y
13. Spinelli AE, D'Ambrosio D, Calderan L, Marengo M, Sbarbati A, Boschi F (2009) Cerenkov radiation allows in vivo optical imaging of positron emitting radiotracers. Phys Med Biol 55:483–495. doi:10.1088/0031-9155/55/2/010
14. Lohrmann C, Zhang H, Thorek DL, Desai P, Zanzonico PB et al (2015) Cerenkov luminescence imaging for radiation dose calculation of a 90Y-labeled gastrin-releasing peptide receptor antagonist. J Nucl Med 56:805–811. doi:10.2967/jnumed.114.149054
15. Allison J, Amako K, Apostolakis J, Araujo H, Dubois PA et al (2006) Geant4 developments and applications. IEEE T Nucl Sci 53:270–278. doi:10.1109/TNS.2006.869826
16. Agostinelli S, Allison J, Amako KA, Apostolakis J, Araujo H, Arce P et al (2003) GEANT4—a simulation toolkit. Nucl Instrum Meth A 506:250–303. doi:10.1016/S0168-9002(03)01368-8
17. Geng C, Tang X, Hou X, Shu D, Chen D (2014) Development of Chinese hybrid radiation adult phantoms and their application to external dosimetry. Sci China Technol Sci 57:713–719. doi:10.1007/s11431-014-5480-x

18. International Commission on Radiation Units and Measurements (ICRU) Photon, Electron, Proton and Neutron Interaction Data for Body Tissues (1992). ICRU Report 46
19. International Commission on Radiological Protection (ICRP) Basic anatomical and physiological data for use in radiological protection reference values (2002). ICRP Publication 89, Ann ICRP 32
20. Bashkatov AN, Genina EA, Kochubey VI, Tuchin VV (2005) Optical properties of human skin, subcutaneous and mucous tissues in the wavelength range from 400 to 2000 nm. J Phys D 38:2543–2555. doi:10.1088/0022-3727/38/15/004
21. Bashkatov AN, Genina EA, Tuchin VV (2011) Optical properties of skin, subcutaneous, and muscle tissues: a review. J Innov Opt Heal Sci 4:9–38. doi:10.1142/S1793545811001319
22. Helo Y, Rosenberg I, D'Souza D, MacDonald L, Speller R, Royle G, Gibson A (2014) Imaging Cerenkov emission as a quality assurance tool in electron radiotherapy. Phys Med Biol 59:1963–1978. doi:10.1088/0031-9155/59/8/1963
23. Klein JS, Mitchell GS, Cherry SR (2017) Quantitative assessment of Cerenkov luminescence for radioguided brain tumor resection surgery. Phys Med Biol 62:4183–4201. doi:10.1088/1361-6560/aa6641
24. Zhang R, Fox CJ, Glaser AK, Gladstone DJ, Pogue BW (2013) Superficial dosimetry imaging of Čerenkov emission in electron beam radiotherapy of phantoms. Phys Med Biol 58:5477–5493. doi:10.1088/0031-9155/58/16/5477
25. Andreozzi JM, Zhang R, Gladstone DJ, Williams BB, Glaser AK, Pogue BW, Jarvis LA (2016) Cherenkov imaging method for rapid optimization of clinical treatment geometry in total skin electron beam therapy. Med Phys 43:993–1002. doi:10.1118/1.4939880
26. Zhang R, Glaser AK, Gladstone DJ, Fox CJ, Pogue BW (2013) Superficial dosimetry imaging based on Čerenkov emission for external beam radiotherapy with megavoltage X-ray beam. Med Phys 40:101914. doi:10.1118/1.4821543
27. Jang KW, Yagi T, Pyeon CH, Yoo WJ, Shin SH, Jeong C, Min BJ, Shin D, Misawa T, Lee B (2013) Application of Cerenkov radiation generated in plastic optical fibers for therapeutic photon beam dosimetry. J Biomed Opt 18:027001. doi:10.1117/1.JBO.18.2.027001
28. Glaser AK, Voigt WH, Davis SC, Zhang R, Gladstone DJ, Pogue BW (2013) Three-dimensional Čerenkov tomography of energy deposition from ionizing radiation beams. Opt Lett 38:634–636